J. Hydrol. Hydromech., 69, 2021, 1, 98–107
DOI: 10.2478/johh-2020-0045
ISSN 1338-4333

sciendo Journal of Hydrology and Hydromechanics

Effect of T-shaped spur dike length on mean flow characteristics along a 180-degree sharp bend

Maryam Akbari[1], Mohammad Vaghefi[1*], Yee-Meng Chiew[2]

[1] Department of Civil Engineering, Persian Gulf University, Shahid Mahini Street, 7516913817, Bushehr, Iran. Emails: m.akbari@pgu.ac.ir, Vaghefi@pgu.ac.ir
[2] Department of Civil and Environmental Engineering, Nanyang Technological University, 639798, Singapore. E-mail: cymchiew@ntu.edu.sg
[*] Corresponding author. Tel.: (+98) 77-31222401. Fax: (+98) 77-33440376. E-mail: Vaghefi@pgu.ac.ir

Abstract: An open channel flume with a central 180-degree bend with a rigid bed is designed to obtain a better understanding of the complex flow pattern around a T-shaped spur dike located in a sharp bend. The 3-dimensional velocities are measured by using an acoustic Doppler velocimetry under clear-water conditions. This study's primary objective is to compare variations of the mean flow pattern along a 180-degree bend with a variety of T-shaped spur dike lengths. In order to do so, parameters such as streamlines, the maximum velocity distribution, and the secondary flow strength under the influence of three T-shaped spur dike lengths will be analyzed and then compared with the case where no spur dikes are implemented. The results show that with the spur dike placed at the bend apex, the mean secondary flow strength at that range increases by approximately 2.5 times. In addition, a 67% increase in the length of the wing and web of the spur dike leads to a 27% growth in the mean secondary flow strength along the bend.

Keywords: 3-Dimensional velocity; Secondary flows; T-shaped spur dike; Acoustic Doppler velocimetry.

INTRODUCTION

The flow pattern and scouring process along a channel bend are significantly altered by installing a spur dike (Evangelista et al., 2017). Under this condition, the complex secondary currents at the bend are augmented by the 3-dimensional flow field around the spur dike. A review of the literature on this topic reveals the following: (1) very few studies on spur dikes located at bends in comparison to the straight paths have hitherto been conducted; (2) most published studies conducted at bends have focused on straight spur dikes (Fazli et al., 2008; Gill, 1972; Mehraein et al., 2014; Perzedwojski et al., 1995; Sharma and Mohapatra, 2012; Yang et al., 2019); and (3) most studies have centered around scouring and measurements of the maximum scour depth rather than the related flow field.

Ghodsian and Vaghefi (2009) and Vaghefi et al. (2012) are among the first ones to analyze the flow and scour patterns around T-shaped spur dikes in bends. They studied the effect of the length of the spur dike wing and web, spur dike location, the radius of the bend, Froude number, and flow intensity on bed topography variations and the scour depth value under clear-water conditions in a 90-degree bend. Later, the SSIIM numerical model was used to examine submergence ratios' effect on the maximum scour depth variations around T-shaped spur dikes (Vaghefi et al., 2016b). Furthermore, using this numerical model, they investigated the flow pattern around attractive, repelling, and vertical T-shaped spur dikes (Vaghefi et al., 2019b). Also, they used the Flow-3D numerical model to simulate the flow around them in a 90-degree bend (Vaghefi et al., 2018a).

Published literature on spur dikes located in river bends reveals that most of the research has concentrated on the formation of the scour hole and estimation of its maximum depth. Unfortunately, no experimental study has hitherto been done concerning the ensuing flow pattern around the T-shaped spur dikes in a 180-degree sharp bend. To bridge this gap, the present study has incorporated a laboratory study to examine the flow pattern around T-shaped spur dikes, which have the least amount of scour amongst all geometric shapes of spur dikes (Vaghefi et al., 2020) with different lengths in a 180-degree sharp bend. In order to do so, the mean flow pattern parameters such as the streamlines, the maximum velocity distribution, and the secondary flow strength are analyzed under the influence of spur dike wing and web lengths and are compared with the case where no spur dikes are installed in the bend.

EXPERIMENTAL SETUP

The experiments were done in a bent-flume with a central angle of 180 degrees. The flume was located in the Hydraulics Laboratory of Persian Gulf University in Iran. It consisted of a 6.5-meter-long straight reach upstream and a 5.1-meter-long straight reach downstream. It was 70 cm deep and 100 cm wide with a ratio of curvature radius (R) to channel width (B) of 2 (Fig. 1). A picture of the flume with its auxiliary components in the laboratory is illustrated in Fig. 1a. The flume bed was rigid and coated with uniformly distributed sediments with the median diameter = 1.5 mm. Each test was conducted with a constant approach flow depth and discharge. The constant discharge used was 95 L/s. The straight section upstream of the bend had a constant approach flow depth (h) of 20 cm. The approach flow Froude number (Fr) and the flow Reynolds number (Re) were 0.34 and 67857. The Froude and Reynolds numbers were calculated based on the flow upstream of the bend, the middle of the channel width, and immediately before the beginning of the bend. They had almost equal values for all of the tests. In any case, the slight difference of Fr and Re between the tests seems unlikely to affect the results significantly. Besides, all the experiments were carried out under clear-water conditions (Aksoy et al., 2017; Namaee and Sui, 2019), with a velocity ratio of $U/U_c = 0.98$, where U = approach mean flow velocity, and U_c = critical mean velocity for the threshold of bed

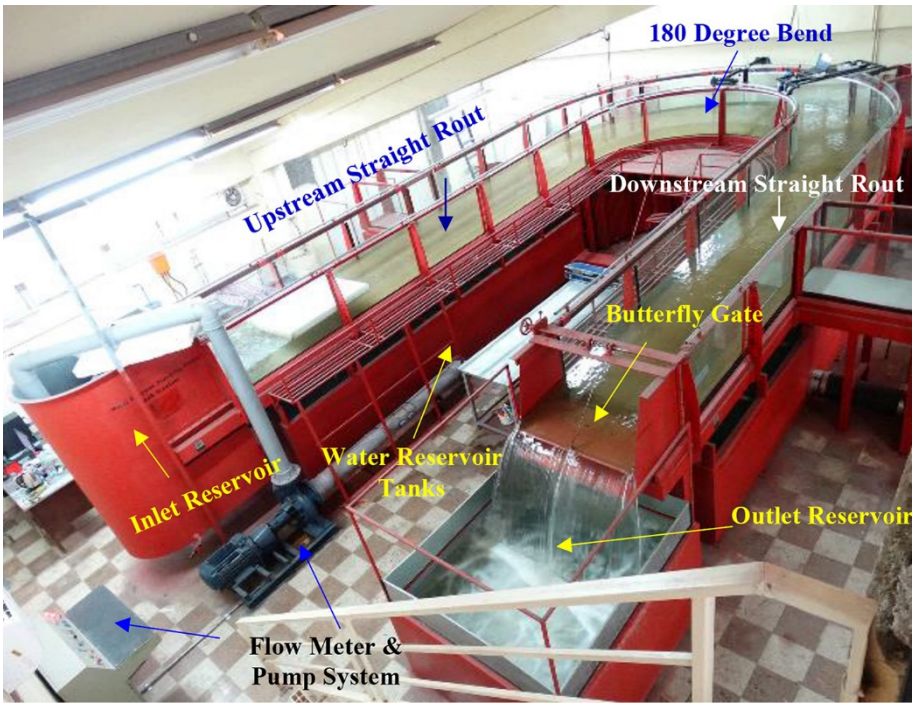

(a)

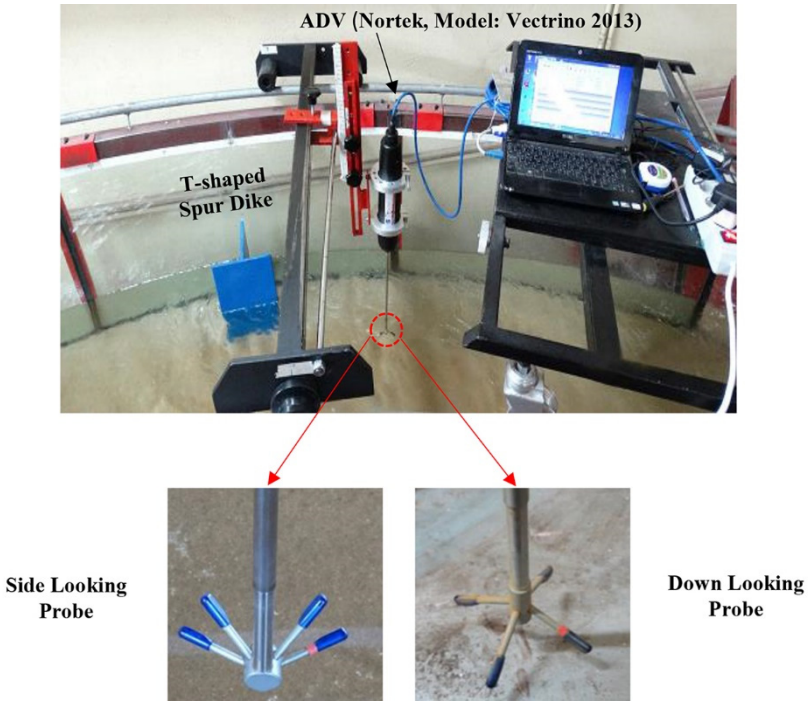

(b)

Fig. 1. Experimental setup used for investigating the flow pattern around the spur dike at the bend: **(a)** Perspective view of the flume and its auxiliary components; **(b)** Location of the T-shaped spur dike and position of Vectrino velocimeter.

sediment entrainment. Based on their experimental works in circular and rectangular channels with different non-cohesive sediments, Novak and Nalluri (1984) proposed the following equation for the computation of U_c:

$$\frac{U_c}{\sqrt{gd_{50}(S_s-1)}} = 0.50\left(\frac{d_{50}}{R}\right)^{-0.40} \quad (1)$$

where d_{50} = median sediment size; R = hydraulic radius; g = gravity acceleration constant; and S_s = specific gravity of sediments.

In this study, U/U_c was selected as 0.98 because it reflected the nearly incipient motion conditions. Conducting tests at $U/U_c \approx 0.98$ is common in scour studies because published data have shown that the maximum local scour depth at hydraulic structures occurs under this condition (Chiew and Melville, 1987; Wu and Chiew, 2012).

Calculating the mean flow velocity is made possible using the measured time-averaged flow velocity components in three different dimensions:

$$U_i = \frac{1}{T}\int_0^T u_i dt \qquad V_i = \frac{1}{T}\int_0^T v_i dt \qquad W_i = \frac{1}{T}\int_0^T w_i dt \tag{2}$$

where (U_i, V_i, W_i) = the mean velocities in the longitudinal, transverse, and vertical directions; and (u_i, v_i, w_i) = the instantaneous velocities.

All the three spur dikes utilized in these tests were made of Plexiglas with a height of 40 cm and a thickness of 1 cm. The geometric dimensions of spur dikes were varied, and they were all T-shaped in the plan view. The spur dikes, which were unsubmerged during the tests, were all installed perpendicular to the channel's outer wall (Vaghefi and Akbari, 2019; Vaghefi et al., 2018b, 2020). The lengths of the web (L) and wing (l) of the three spur dikes tested were the same in every experiment, i.e., $l = L$. The lengths of the three spur dikes were normalized with the channel width, with $L = 0.15B$, $0.2B$, and $0.25B$. The spur dike with $L = 0.15B$ may be considered a short spur dike, while the other two spur dikes are medium. Fig. 2 illustrates a schematic of the laboratory channel's dimensions, spur dikes (Fig. 2a), and the bend's magnified view with its cross sections (Fig. 2b).

Table 1 summarizes the spur dikes' geometry and test conditions, with one test conducted without a spur dike and three with different spur dike lengths. In this table, the logarithmic velocity profile method has been used to calculate the shear velocity. The logarithmic velocity distribution is described by the von Karman-Prandtl equation (Schlichting, 1968):

$$\frac{u}{u*} = \frac{1}{\kappa}\ln\left(\frac{Z}{Z_0}\right) \tag{3}$$

where κ = the von Karman's constant equal to 0.4 (Smart, 1999); Z_0 = the roughness; and u = the mean longitudinal velocity at height Z above the bed.

The equation proposed by Parker et al. (2003) was also used for calculating the critical shear stress. Based on the data obtained from Neill (1968), Parker et al. (2003) modified the Shields equation as follows:

$$\tau_c^* = \frac{1}{2}\left[0.22R_P^{-0.6} + 0.06\exp\left(-17.77R_P^{-0.6}\right)\right] \tag{4}$$

$$R_P = \frac{\sqrt{(s-1)gD_{50}^{\ 3}}}{\nu} \tag{5}$$

where R_P = the particle Reynolds number with a mean diameter of D_{50}; ν = kinematic viscosity of water at 20 °C; s = the relative density ($\frac{\rho_s}{\rho_w}$); and τ_c^* = the Shields critical shear stress under incipient motion conditions.

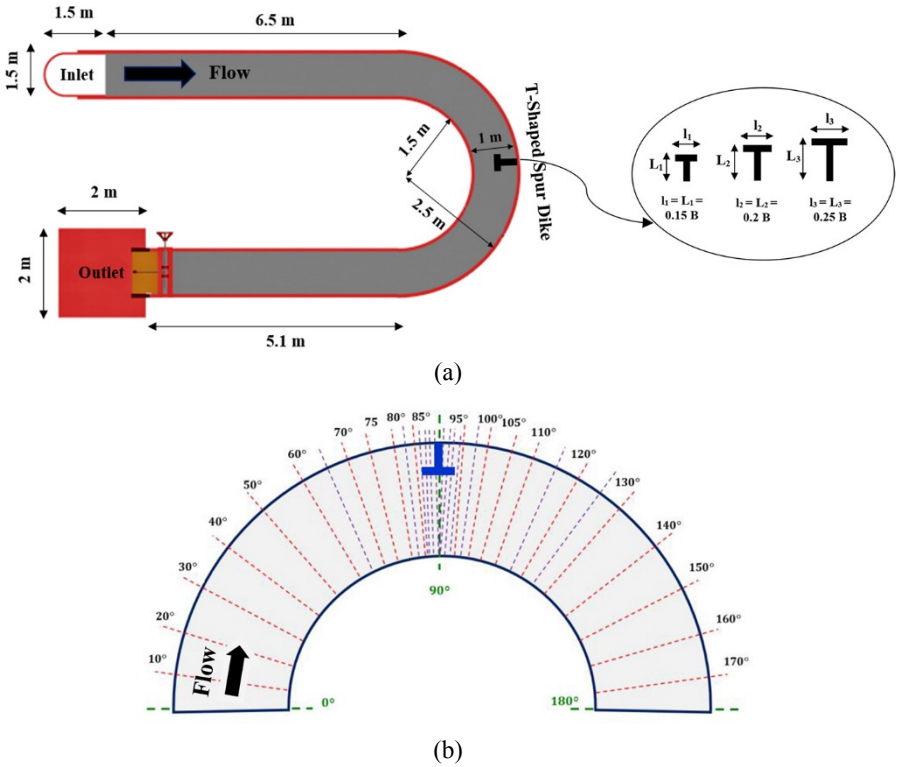

Fig. 2. (a) Schematic plan view of the laboratory flume and spur dikes; **(b)** Magnified view of the bend (not to scale).

Table 1. Summary of the geometry of spur dikes and test conditions of different experimental runs.

Experiment number	Length of spur dike	Flow depth (m)	Critical shear stress	Flow velocity (m/s)	Shear velocity (m/s)
Test 1	…	0.20	0.019	0.395	0.038
Test 2	$L = 0.15B$	0.20	0.019	0.407	0.039
Test 3	$L = 0.2B$	0.20	0.019	0.428	0.041
Test 4	$L = 0.25B$	0.20	0.019	0.441	0.042

A 3-dimensional acoustic Doppler velocimetry (ADV) (Namaee and Sui, 2020; Velísková et al., 2018) was used to measure the 3-dimensional flow field around the T-shaped spur dike in the bend (Vaghefi et al., 2019a). Fig. 1b depicts the down-looking and side-looking probes of the Vectrino and how they were placed along the bend. After placing the ADV in the pre-determined position, we waited for 180 seconds for the flow in the channel and around the ADV probe to stabilize. Then 60 seconds for data collection using the ADV followed, giving a total of 1,500 data points (with a frequency of 25 Hz). The longer time was used in more sensitive areas, such as those near the spur dike and behind the spur dike wing, to obtain more data. Moreover, investigations during the experiment revealed that increasing data collection duration had a negligible effect on the mean flow velocity variations, which is the topic of this study. This has been proved by Sharma and Mohapatra (2012), who conducted tests with ADV using the same frequency of 25 Hz. They found that the mean velocities obtained using periods of 60 or 120 seconds of data collection are essentially the same. In addition, the validity of the data has been checked with the Vectrino software for every collected data by controlling two parameters: Signal-to-Noise Ratio (SNR) and Correlation. Their minimum values, respectively, 20 and 70% were calculated by applying Vectrino and ExplorerV (Nortek, 2009; Vaghefi et al., 2017). After collecting the ADV data and saving them in the Vectrino software, the data were changed in format, filtered, and averaged by using the ExplorerV software (version 1.57, Nortek). This software is capable of modifying the data collected based on the acceleration threshold method. The outlier data can be replaced through linear interpolation or removed from the data as bad samples. It is necessary to point out that these data filtration methods were based on research conducted not only by one of the authors (Vaghefi et al., 2018b) and by other researchers, showing that the results did not have a significant effect on the mean flow pattern. Since the flow velocity data were collected in a relatively long duration, at a sufficient distance from the discharge source and along a large effective length of the channel, the flow was considered a fully developed flow (Jahadi et al., 2019).

With the dimensions of the spur dike taken into consideration, a fine mesh density (0.5–5° interval) around the spur dike and a slightly coarser mesh density (5–10° interval) away from it were employed for data acquisition. Conducting each flow pattern experiment for collecting the flow velocity data using ADV took approximately 20 days. This excludes the time needed to organize, filter, and prepare them for drawing the figures in SigmaPlot and Tecplot 360. After drawing different figures in different sections, more time was required for analyzing the data. In total, each set of experiment took an average of 1.5 to 2 months.

RESULTS AND DISCUSSION

Streamlines

Since the spur dike length significantly affects the lateral flow pattern, the streamlines (Zhang et al., 2020) at different cross sections (at 60°, 89°, 91°, and 150°) are shown in Figs. 3–5 for the three different spur dike lengths ($L = 0.15B$, $L = 0.2B$, and $L = 0.25B$), respectively, to reveal the changes. In these figures, Y and Z are the lateral and vertical axes, respectively.

Fig. 3a clearly shows the formation of a clockwise vortex (A) at the inner wall when the flow passes the 60-degree cross section. This vortex is observed in all three spur dikes tested regardless of their lengths (see Figs. 3a, 4a, and 5a). A point to note is that a similar vortex is also observed to form at the same location in the absence of the spur dike (Vaghefi et al., 2016a). This vortex's generation may be attributed to the presence of a large transverse pressure gradient at this location (near the inner wall) as the water flows around the 180-degree sharp bend (Vaghefi et al., 2016a). The streamlines in Figs. 3a, 4a, and 5a reveal that lengthening the spur dike wing and web causes the clockwise vortex to move closer to the inner wall. Moreover, a secondary counterclockwise vortex (B) appears near the outer wall at levels close to the water surface (see Figs. 4a and 5a). Blanckaert and Graf (2001) reported the generation of such a vortex near the channel's outer wall at the 60-degree cross section in a 120-degree bend in the absence of a spur dike. The difference is that their observed vortex forms near the bed rather than near the water surface. However, the study of Fazli et al. (2008) on flows around a straight spur dike in a 90-degree bend indicated that apart from the vortices that formed at the upstream and downstream ends of the spur dike, a secondary vortex was generated at the 75-degree cross section near the water surface.

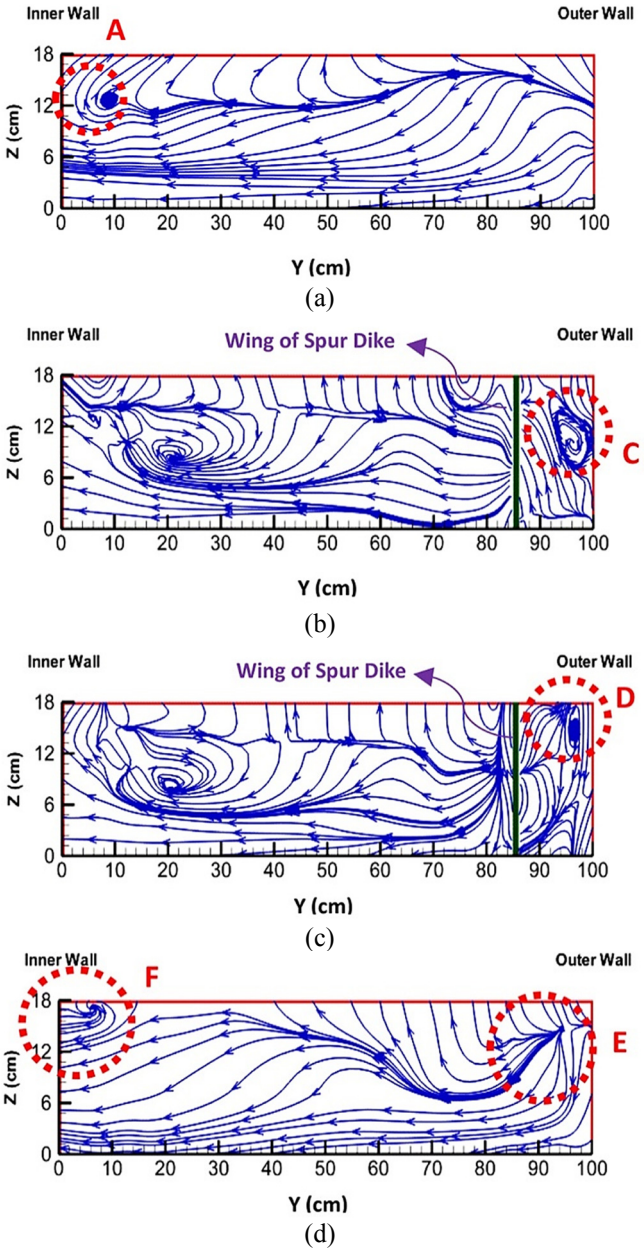

Fig. 3. Streamlines at different cross sections along the 180-degree bend with a T-shaped spur dike for $L = 0.15B$, at: **(a)** 60; **(b)** 89; **(c)** 91; **(d)** 150-degree cross sections.

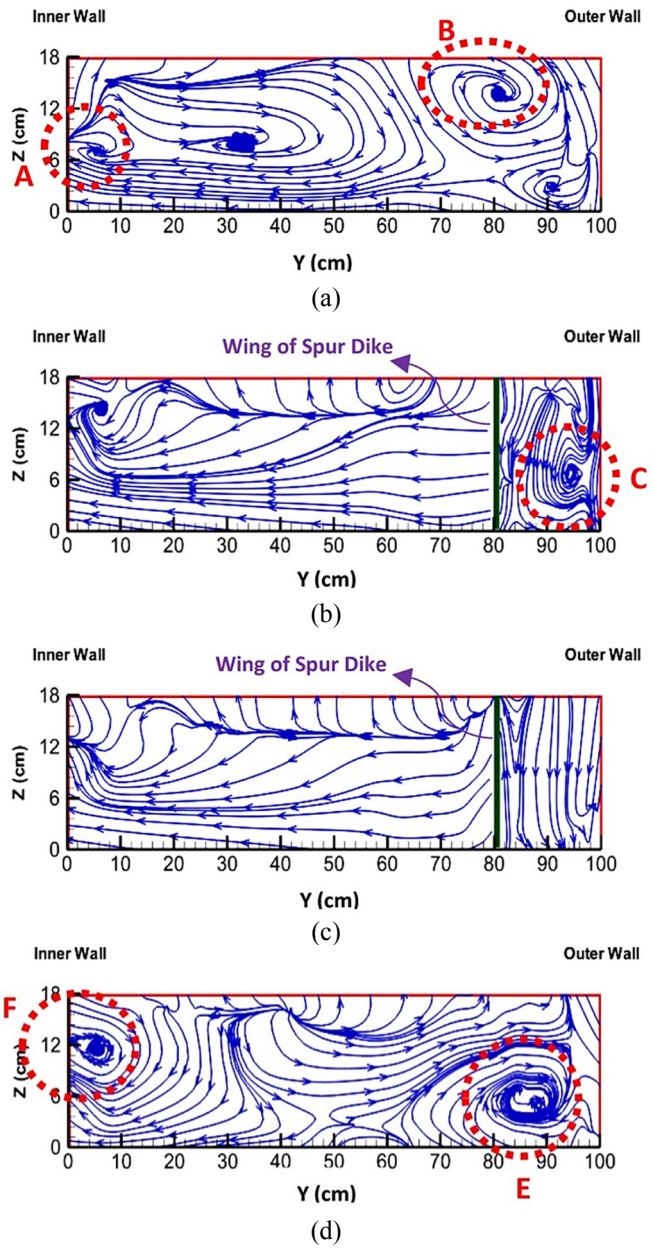

Fig. 4. Streamlines at different cross sections along the 180-degree bend with a T-shaped spur dike for $L = 0.2B$, at: **(a)** 60; **(b)** 89; **(c)** 91; **(d)** 150-degree cross sections.

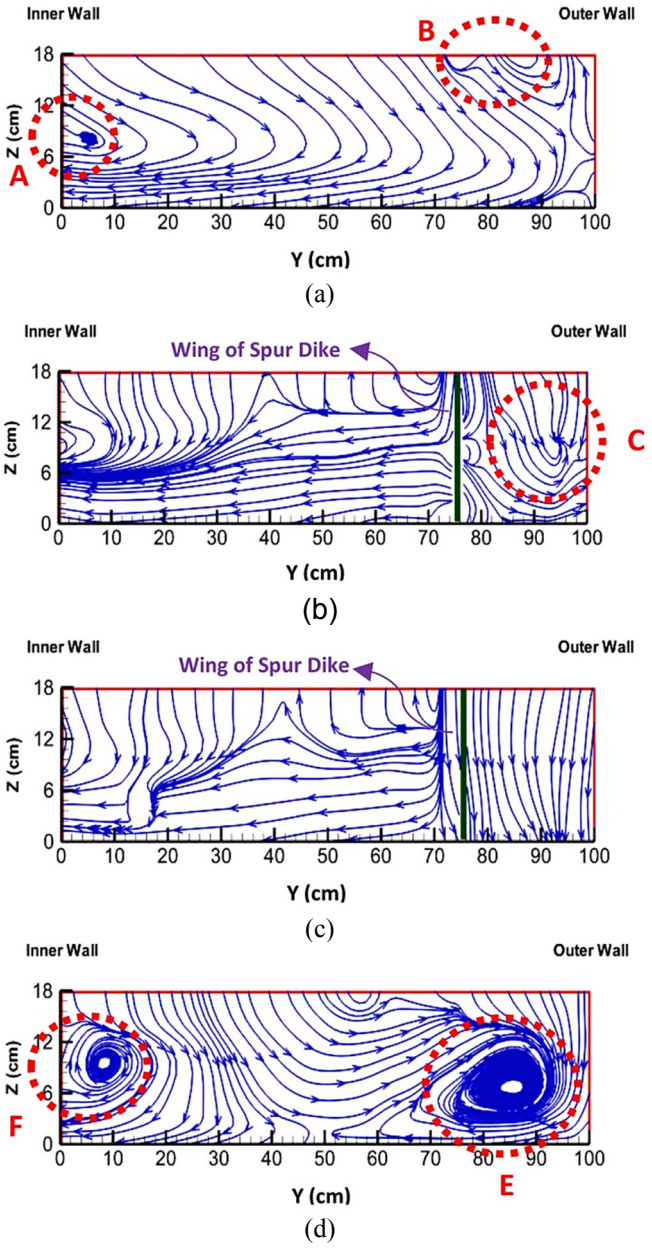

Fig. 5. Streamlines at different cross sections along the 180-degree bend with a T-shaped spur dike for $L = 0.25B$, at: **(a)** 60; **(b)** 89; **(c)** 91; **(d)** 150-degree cross sections.

As the flow approaches the spur dike, apart from the vortex generated at the inner wall, another counterclockwise vortex owing its formation to the returned flow affected by the spur dike is also created behind the spur dike wing (Vortex C in Figs. 3b, 4b, and 5b). As shown in Fig. 3b, the streamlines are extended along the wing wall after hitting the outer wall. As a result, a downflow is generated, resulting in the formation of the observed clockwise vortex. By lengthening the spur dike wing and web by 33% (Fig. 4b), the downflow lines appear counterclockwise because they are under the collision's influence with the spur dike wing. In Fig. 5b, a 67% increase in the area between the wing and the outer wall causes the streamlines to collide with the spur dike web with almost no contact with the wing. Therefore, given the downflow orientation of the stream, a counterclockwise vortex is formed. From this observation, it may be inferred that increasing the space between the wing and the outer wall of the channel causes the downflow streamlines to collide with the spur dike web without hitting the wing, redirecting the flow and forming the counterclockwise vortex. It can then be surmised that lengthening the spur dike wing and web can increase this vortex's dimensions by approximately 7%.

The flow patterns immediately downstream of the spur dike are shown in Figs. 3c, 4c, and 5c. Fig. 3c depicts how a small clockwise vortex is generated in the spur dike's lee with its center located at a depth of approximately 80% of the flow depth (Vortex D). The data in Figs. 4c and 5c show that further constriction of the flow cross section has nullified its formation, and only downward flow is present with streamlines directly impinging onto the channel bed. Therefore, it may be inferred that serious scouring is likely to occur here.

A close examination of the streamlines near the bend exit shows the presence of increasingly stronger secondary flows when the spur dike is lengthened. Figs. 3d, 4d, and 5d evidently display the formation of clockwise vortices near both the inner and the outer walls (zones E and F), with each spur dike ex-

tending to the channel mid-width. This is because the effect of such spur dikes on the flow field is no longer evident at the downstream side of the bend outlet. In summary, the spur dike's presence at a 180-degree bend causes changes to the formation of the secondary vortices in general, making the center of the secondary vortices move closer to the bed. An important inference of this behavior is that such a situation can potentially cause the formation of a deeper scour hole. This inference is confirmed by the study of Fazli et al. (2008) measuring an increase of the scour depth associated with lengthening a straight spur dike in a 90-degree bend under clear-water conditions.

The streamline patterns near the free surface and bed of the three spur dike lengths tested and their respective magnified illustrations are shown in Figs. 6–8. In these figures, X denotes the longitudinal axis. A comparison of Figs. 6–8 reveals that the streamlines are oriented towards the inner wall close to the bed, whereas at the layer near the water surface, the streamlines are directed towards the bend's outlet without collision with the inner wall. This is similar to the flow pattern without a spur dike (Vaghefi et al., 2016a). Moreover, the present experimental results bear a close resemblance with those reported by Abhari et al. (2010) in terms of streamlines variations of the secondary flow. Lengthening the dike wing and web tends to direct the flow towards the channel mid-width, which causes more flow to move towards the bed at the inner wall. This is observed from the second half of the bend.

Based on Figs. 6a, b, 7a, b, and 8a, b, the counterclockwise vortex at the near-bed region is enlarged as one moves farther downstream from the spur dike due to additional constriction of the cross section (see Vortex A). It is noteworthy that in the experimental work of Safarzadeh et al. (2016), this vortex is not fully formed near the bed with the flow pattern around either straight or T-shaped spur dikes even though the channel width and the spur dike length used in their study are similar to those of the present study. They used three different spur dikes (one straight and two T-shaped) with 15% of the channel width (with the length of one T-shaped spur dike wing = half of the web). The most plausible reason is that their channel was straight, but the channel used in the present study has a 180-degree sharp bend, causing stronger secondary flows.

A point to note here is that no patently clear vortex is visible near the water surface at the upstream side of the short spur dike (Fig. 6). This is probably due to the absence of the return flow, which induces the formation of a counterclockwise vortex (at higher water levels in both areas B and C, see Fig. 8) with the longer spur dike. Ghodsian and Vaghefi (2009) observed the formation of two counterclockwise vortices at the upstream and downstream sides of a T-shaped spur dike installed at the 75-degree cross section in a 90-degree bend. In other words, the dimensions of the flow separation zone along with the length of the flow reattachment zone increase with the length of the spur dike wing and web. It may be surmised from Figs. 7b, d and 8b, d that the formation of another counterclockwise vortex in front of the wing is associated with the strong return flows induced by the spur dikes with $L = 0.2B$ and $L = 0.25B$ (Vortex D). This phenomenon may be induced by the interaction between the flows in a sharp bend and those influenced by the spur dike located in the channel since the spur dike's presence has reduced the cross-sectional area there.

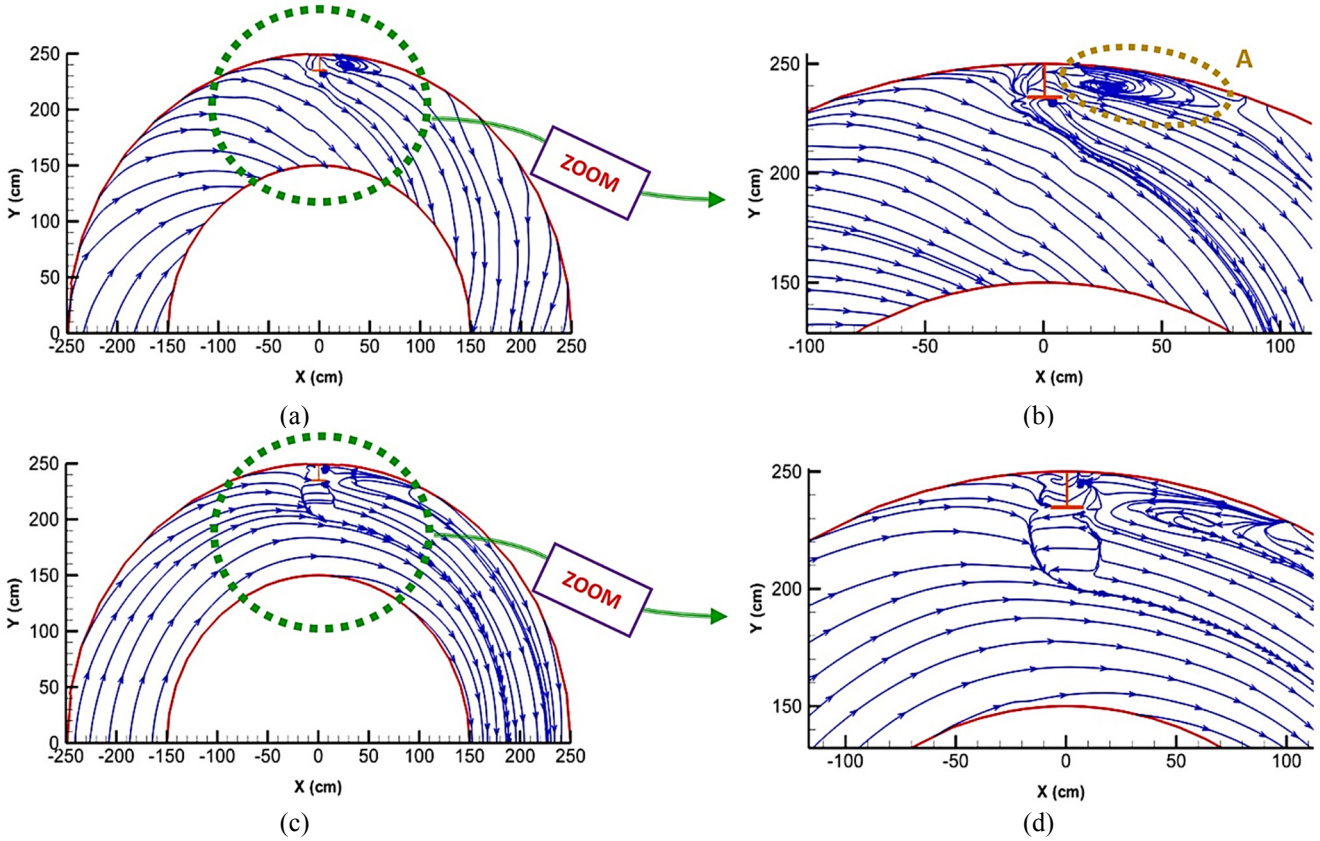

Fig. 6. Streamline patterns in different sections of the 180-degree bend with a T-shaped spur dike with $L = 0.15B$: **(a)** at a distance of 5% of the flow depth from the bed (near-bed); **(b)** a magnified illustration of **(a)**; **(c)** at a distance of 95% of the flow depth from the bed (near-surface); **(d)** a magnified illustration of **(c)**.

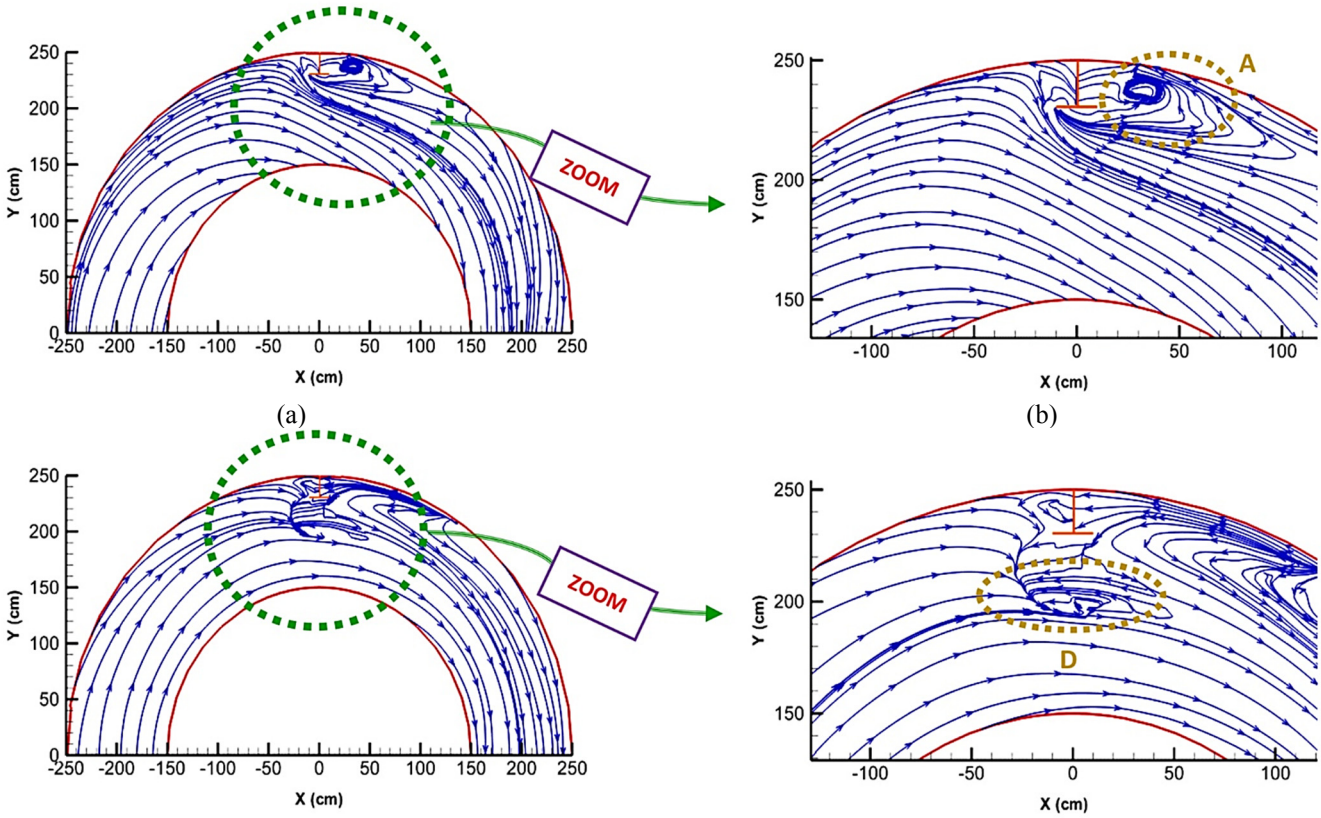

Fig. 7. Streamline patterns in different sections of the 180-degree bend with a T-shaped spur dike with $L = 0.2B$: **(a)** at a distance of 5% of the flow depth from the bed (near-bed); **(b)** a magnified illustration of **(a)**; **(c)** at a distance of 95% of the flow depth from the bed (near-surface); **(d)** a magnified illustration of **(c)**.

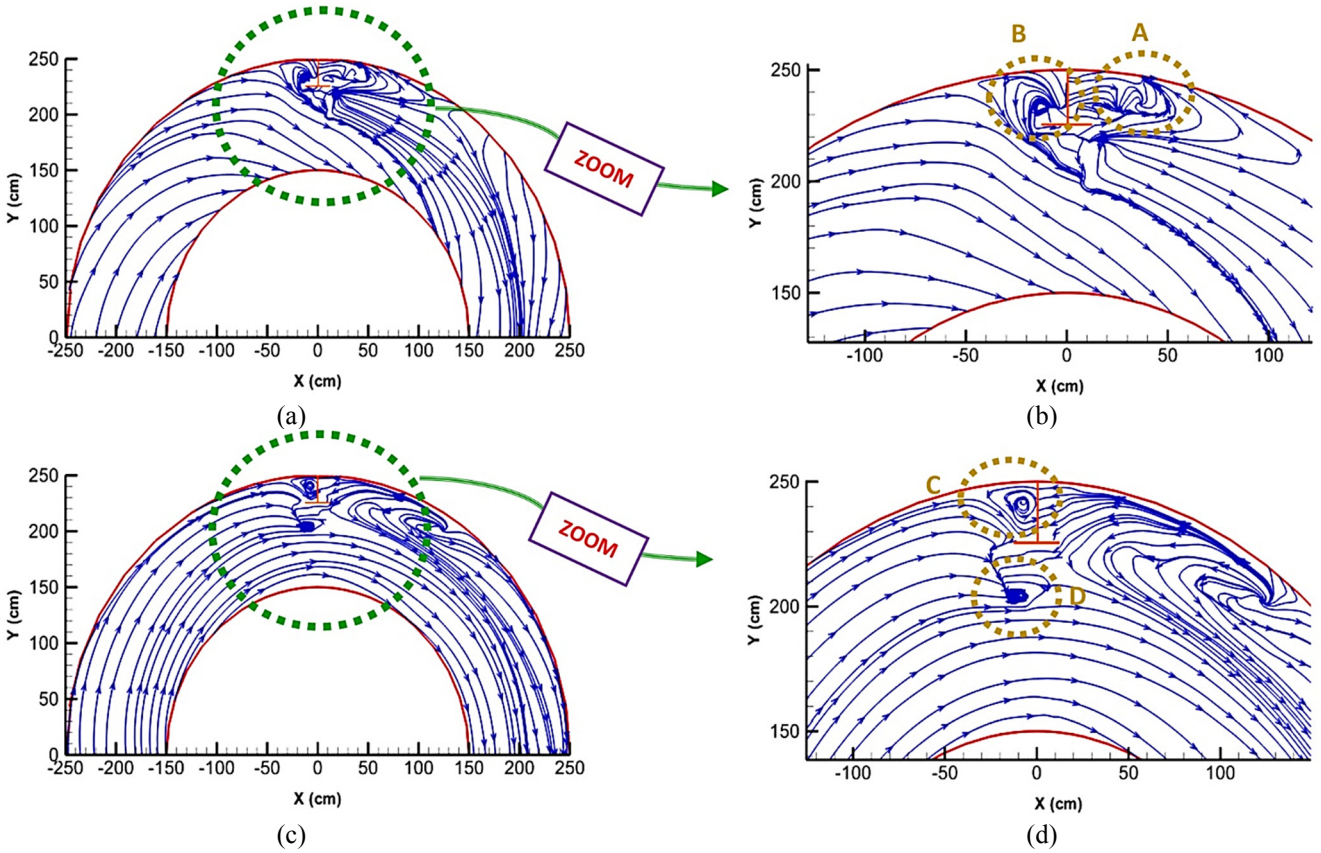

Fig. 8. Streamline patterns in different sections of the 180-degree bend with a T-shaped spur dike with $L = 0.25B$: **(a)** at a distance of 5% of the flow depth from the bed (near-bed); **(b)** a magnified illustration of **(a)**; **(c)** at a distance of 95% of the flow depth from the bed (near-surface); **(d)** a magnified illustration of **(c)**.

Maximum flow velocity

The maximum flow velocity distribution along the bend in every case tested is presented in Fig. 9. The data show that the spur dikes' constriction effect causes the maximum flow velocity to move towards the inner wall at the layer near the bed (Fig. 9a). This is a key factor in preventing erosion at the outer walls of the channel. According to a previous study conducted by Vaghefi et al. (2016a) on a 180-degree sharp bend with no spur dikes, it is noted that the maximum flow velocity is moved to the outer wall upon reaching the downstream half of the bend. At the upstream half of the bend, the spur dike causes no significant changes on the maximum velocity locus because the maximum velocities through the bend without a spur dike also occur near the inner wall. A closer examination of the layer close to the water surface (see Fig. 9b) reveals that the flow is re-directed towards the outer wall with the maximum flow velocity completely re-oriented by the spur dike. Fig. 9b shows how the maximum near-surface velocity moves towards the inner wall due to lengthening the wing and web of the spur dike. Herein, the longest spur dike's influence on changes of the maximum flow velocity is patently evident, making spur dike installation such an excellent scour countermeasure against erosion at the outer wall of bends. It is also considerable with regards to the maximum flow velocity variations at the layer near the bed and that near the water surface because installing spur dikes respectively equal to 15, 20, and 25% of the channel width increases the maximum flow velocity at the layer near the bed by 40, 67, and 77%, and that at the layer near the water surface by 16, 27, and 38% in comparison to the case without a spur dike.

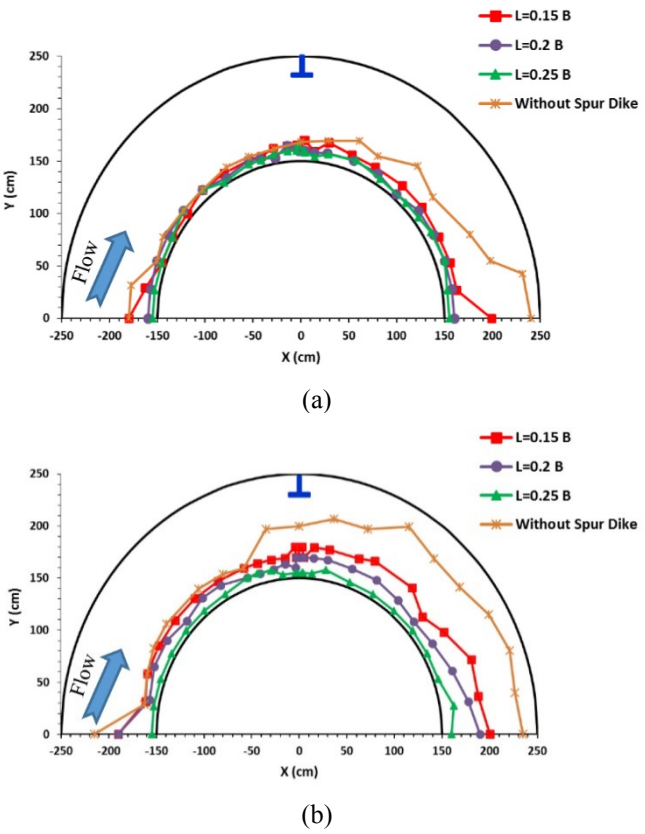

Fig. 9. Distribution of the maximum flow velocity in cases with and without a T-shaped spur dike at a distance of: **(a)** 5% (near-bed); **(b)** 95% (near-surface) of the flow depth from the bed.

Secondary flow strength

The study of the secondary flow strength in meandering rivers is of great importance since the generation of secondary flows indicates that the secondary flows in a meandering channel are more intensive than those in a straight channel due to their contributions centrifugal forces (Liu et al., 2018). Showing the secondary flow strength results computed by using the method proposed by Shukry (1950), Fig. 10 reveals that the secondary flow strengths of the three different spur dikes along the upstream half of the bend (up to 70 degrees) do not differ significantly. Nonetheless, they are still nearly 60% higher than that without a spur dike. Lengthening the spur dike can cause the secondary flow strength to increase by a value of up to 27% at the bend apex. Consequently, the bed shear stress increases, and the corresponding scour that accompanies a longer spur dike clearly cannot be ignored. This was studied with straight spur dikes located in a straight channel by Koken and Gogus (2015). They found that the maximum shear stress and pressure that form at the upstream nose of the spur dikes increased if the length of the spur dike increased. In Fig. 10, however, the secondary flow strength around the bend apex of the spur dike, regardless of its length, reaches about 2.5 times that of the

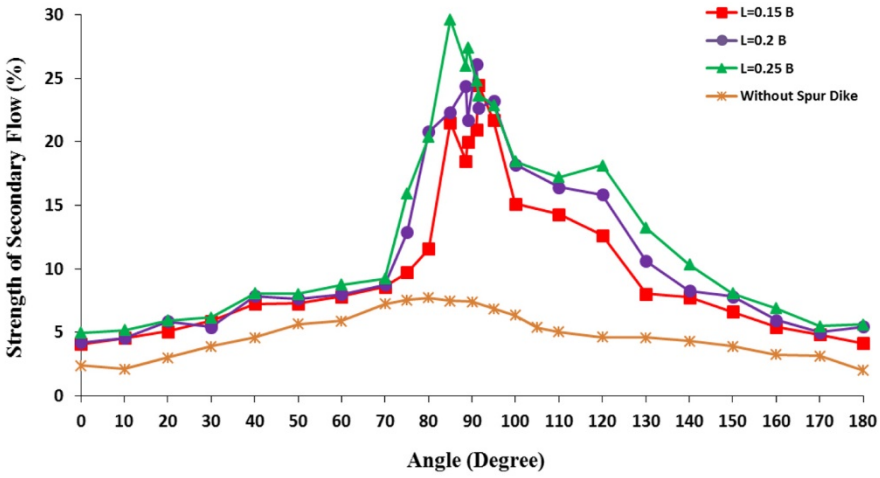

Fig. 10. Variations of the secondary flow strength in different cross sections along the 180-degree bend with and without a T-shaped spur dike.

bend without a spur dike. This is indicative of the important effect of the spur dike on the secondary flow strength. In the downstream half of the bend, the secondary flow strength remains higher for cases with a spur dike, with the largest increment for the longest dike. In summary, it may be inferred that the mean secondary flow strengths in the downstream half of the bend are 5, 11, 12.5, and 14%, respectively, for cases without a spur dike, and when L = 0.15B, 0.2B, and 0.25B. The increase and decrease of the secondary flow strength, respectively associated with the upstream and downstream halves of the bend (see Fig. 10), were also observed by Rozovskii (1957). According to the experimental data obtained from tests conducted with a T-shaped spur dike in a 90-degree bend by Vaghefi (2009), the average increase of the secondary flow strength of the spur dike with a length equal to 20% of the channel width at the 75-degree position is approximately 8% compared to that with a length equal to 15% of the channel width. In this study, which is conducted in a 180-degree bend, this value is 15%. The present data are in complete agreement with Shukry (1950) and Lien et al. (1999), who stated that the secondary flow in a sharp bend was higher than that of a milder bend. In another study, Vaghefi et al. (2015) compared the secondary flow strength numerically along a 90-degree bend of varying curvature radii with a T-shaped spur dike using the method incorporated in Shukry (1950). They found that the maximum secondary flow strength was generated along a sharp bend (R/B = 2) under submerged or unsubmerged spur dike conditions.

CONCLUSIONS

Considering the lack of work done on the effect of T-shaped spur dikes on flow patterns in 180-degree sharp bends in the literature, the present work measured the 3D flow velocities with such dikes in a 180-degree bend by using an ADV to measure the mean flow patterns while lengthening the spur dike wing and web. The mean flow pattern parameters, such as the streamlines at the transverse and vertical sections, the maximum velocity distribution, and the secondary flow strength in the bend, were determined and compared with the case without a spur dike. The following conclusions are drawn from the study:

1. A clockwise vertical vortex is formed at the 60-degree cross section of the three spur dikes tested. The center of the vortex, located at a distance of ~5% of the channel width from the inner wall, is located closer to the inner wall with the longer dike.
2. Due to the high flow turbulence associated with the spur dike's influence, the flow undergoes a number of changes in the area behind the upstream wing of the spur dike. Consequently, another small vortex is formed at this section near the inner wall in addition to that described earlier. Increasing the spur dike wing and web lengths from 0.15B to 0.25B increases the dimensions of this vortex by approximately 7%.
3. Up to the bend exit, the flow is still influenced by the spur dike, with the core of the vortex moving towards the bed when the spur dike constricts the cross section.
4. The spur dike's effect with a length equal to 25% of the channel width on the displacement of the maximum flow velocities is very pronounced, which has the possibility of offering protection and stability on the outer wall against erosion.
5. Installing spur dikes equal to 15, 20, and 25% of the channel width, respectively, increases the maximum flow velocity at the layer near the bed by 40, 67, and 77% and that at the layer near the water surface by 16, 27, and 38% in comparison with the case where no spur dikes are installed.
6. The mean secondary flow strength is ~2.5 times stronger than that at a bend without a spur dike provided that the dike is placed at the bend apex.
7. Placing a longer spur dike causes a 27% increase (compared to the shortest spur dike tested) in the mean secondary flow strength within the spur dike area.

REFERENCES

Abhari, M.N., Ghodsian, M., Vaghefi, M., Panahpur, N., 2010. Experimental and numerical simulation of flow in a 90 bend. Flow. Meas. Instrum., 21, 292–298. https://doi.org/10.1016/j.flowmeasinst.2010.03.002

Aksoy, A.O., Bombar, G., Arkis, T., Guney, M.S., 2017. Study of the time-dependent clear water scour around circular bridge piers. J. Hydrol. Hydromech., 65, 26–34. https://doi.org/10.1515/johh-2016-0048

Blanckaert, K., Graf, W.H., 2001. Mean flow and turbulence in open-channel bend. J. Hydraul. Eng., 127, 835–847. https://doi.org/10.1061/(ASCE)0733-9429(2001)127:10(835)

Chiew, Y.M., Melville, B.W., 1987. Local Scour around Bridge Piers. J. Hydraul. Res., 25, 15–26. https://doi.org/10.1080/00221688709499285

Evangelista, S., Giovinco, G., Kocaman, S., 2017. A multi-parameter calibration method for the numerical simulation of morphodynamic problems. J. Hydrol. Hydromech., 65, 175–182. https://doi.org/10.1515/johh-2017-0014

Fazli, M., Ghodsian, M., Salehi Neyshabouri, S.A.A., 2008. Scour and flow field around a spur dike in a 90^{o} bend. Int. J. Sediment. Res., 23, 56–68. https://doi.org/10.1016/S1001-6279(08)60005-0

Ghodsian, M., Vaghefi, M., 2009. Experimental study on scour and flow field in a scour hole around a T-shape spur dikes in a 90˚ bend. Int. J. Sediment. Res., 24, 145–158. https://doi.org/10.1016/S1001-6279(09)60022-6

Gill, M.A., 1972. Erosion and sand beds around spur dikes. J. Hydraul. Div., 98, 1587–1602.

Jahadi, M., Afzalimehr, H., Rowinski, P.M., 2019. Flow structure within a vegetation patch in a gravel-bed river. J. Hydrol. Hydromech., 67, 154–162. https://doi.org/10.2478/johh-2019-0001

Koken, M., Gogus, M., 2015. Effect of spur dike length on the horseshoe vortex system and the bed shear stress distribution. J. Hydraul. Res., 53, 196–206. https://doi.org/10.1080/00221686.2014.967819

Lien, H.C., Hsieh, T.Y., Yang, J.C., Yeh, K.C., 1999. Bend-flow simulation using 2D depth-averaged model. J. Hydraul. Eng., 125, 1097–1108. https://doi.org/10.1061/(ASCE)0733-9429(1999)125:10(1097)

Liu, X., Zhou, Q., Huang, S., Guo, Y., Liu, C., 2018. Estimation of flow direction in meandering compound channels. J. Hydrol., 556, 143–153. https://doi.org/10.1016/j.jhydrol.2017.10.071

Mehraein, M., Ghodsian, M., Najibi, S.A., 2014. Experimental investigation on the flow field around a spur dike in a 90 degree sharp bend. In: Proc. of River flow Conf., Lausanne, pp. 743–749.

Namaee, M.R., Sui, J., 2019. Impact of armour layer on the depth of scour hole around side-by-side bridge piers under ice-covered flow condition. J. Hydrol. Hydromech., 67, 240–251. https://10.2478/johh-2019-0010

Namaee, M.R., Sui, J., 2020. Velocity profiles and turbulence intensities around side-by-side bridge piers under ice-covered flow condition. J. Hydrol. Hydromech., 68, 70–82. https://10.2478/johh-2019-0029

Neill, C.R., 1968. A re-examination of the beginning of movement for coarse granular bed materials. Hydraulics Research Station, Wallingford.

Nortek, A.S., 2009. Vectrino velocimeter manual. Nortek AS, Bærum.

Novak, P., Nalluri, C., 1984. Incipient motion of sediment particles over fixed beds. J. Hydraul. Res., 22, 181–197. https://doi.org/10.1080/00221688409499405

Parker, G., Toro-Escobar, C.M., Ramey, M., Beck, S., 2003. Effect of floodwater extraction on mountain stream morphology. J. Hydral. Eng., 129, 885–895. https://doi.org/10.1061/(ASCE)0733-9429(2003)129:11(885)

Perzedwojski, B., Blazejewski, R., Pilarczyk, K.W., 1995. River Training Techniques: Fundamental, Design and Application. A.A. Balkema, Rotterdam.

Rozovskii, I.L., 1957. Flow of water in bends of open channels, Academy of Sciences of the Ukrainian SSR, Kiev.

Safarzadeh, A., Salehi Neyshabouri, S.A.A., Zarrati, A.R., 2016. Experimental investigation on 3D turbulent flow around straight and T-shaped groynes in a flat bed channel. J. Hydraul. Eng., 142, 04016021. https://doi.org/10.1061/(ASCE)HY.1943-7900.0001144

Schlichting, H., 1968. Boundary Layer Theory. McGraw-Hill, New York.

Sharma, K., Mohapatra, P.K., 2012. Separation zone in flow past a spur dyke on rigid bed meandering channel. J. Hydraul. Eng., 138, 897–901. https://doi.org/10.1061/(ASCE)HY.1943-7900.0000586

Shukry, A., 1950. Flow around bends in an open flume. T. Am. Soc. Civ. Eng., 115, 751–779.

Smart, G.M., 1999. Turbulent velocity profiles and boundary shear in gravel bed rivers. J. Hydral. Eng., 125, 106–116. https://doi.org/10.1061/(ASCE)0733-9429(1999)125:2(106)

Vaghefi, M., 2009. Experimental investigation on flow field and scour pattern around T-shape spur dikes in a 90° bend. Ph.D. Thesis, Tarbiat Modares University, Tehran.

Vaghefi, M., Akbari, M., 2019. Procedure for setting up 180 degree sharp bend flume including construction and examinations with hydraulic structures. Sci. Iran., 26, 270–278. https://doi.org/10.24200/sci.2018.5033.1054

Vaghefi, M., Ghodsian, M., Salehi Neyshabouri, S.A.A., 2012. Experimental study on scour around a T-shaped spur dike in a channel bend. J. Hydraul. Eng., 27, 498–509. https://doi.org/10.1061/(ASCE)HY.1943-7900.0000536

Vaghefi, M., Safarpoor, Y., Hashemi, S.S., 2015. Effects of relative curvature on the scour pattern in a 90° bend with a T-shaped spur dike using a numerical method. Int. J. River. Basin. Manage., 13, 501–514. https://doi.org/10.1080/15715124.2015.1049181

Vaghefi, M., Akbari, M., Fiouz, A.R., 2016a. An Experimental study of mean and turbulent flow in a 180 degree sharp open channel bend: secondary flow and bed shear stress. KSCE. J. Civ. Eng., 20, 1582–1593. https://doi.org/10.1007/s12205-015-1560-0

Vaghefi, M., Safarpoor, Y., Akbari, M., 2016b. Numerical investigation of flow pattern and components of three-dimensional velocity around a submerged T-shaped spur dike in a 90 degree bend. J. Cent. South. Univ., 23, 2984–2998. https://doi.org/10.1007/s11771-016-3362-z

Vaghefi, M., Ghodsian, M., Akbari, M., 2017. Experimental investigation on 3D flow around a single T-shaped spur dike in a bend. Period. Polytech-Civ., 61, 462–470. https://doi.org/10.3311/PPci.7999

Vaghefi, M., Faraji, B., Akbari, M., Eghbalzadeh, A., 2018a. Numerical investigation of flow pattern around a T-shaped spur dike in the vicinity of attractive and repelling protective structures. J. Braz. Soc. Mech. Sci., 40, 93. https://doi.org/10.1007/s40430-017-0954-y

Vaghefi, M., Mahmoodi, K., Akbari, M., 2018b. A comparison among data mining algorithms for outlier detection using flow pattern experiments. Sci. Iran., 25, 590–605. https://doi.org/10.24200/sci.2017.4182

Vaghefi, M., Mahmoodi, K., Akbari, M., 2019a. Detection of outlier in 3D flow velocity collection in an open-channel bend using various data mining techniques. IJST-T Civ. Eng., 43, 197–214. https://doi.org/10.1007/s40996-018-0131-2

Vaghefi, M., Radan, P., Akbari, M., 2019b. Flow pattern around attractive, vertical, and repelling t-shaped spur dikes in a mild bend using CFD modeling. Int. J. Civ. Eng., 17, 607–617. https://doi.org/10.1007/s40999-018-0340-x

Vaghefi, M., Mahmoodi, K., Setayeshi, S., Akbari, M., 2020. Application of artificial neural networks to predict flow velocity in a 180° sharp bend with and without a spur dike. Soft. Comput., 24, 8805–8821. https://doi.org/10.1007/s00500-019-04413-5

Velísková, Y., Chára, Z., Schügerl, R., Dulovičová, R., 2018. CFD simulation of flow behind overflooded obstacle. J. Hydrol. Hydromech., 66, 448–456. https://doi.org/10.2478/johh-2018-0028

Wu, Y.S., Chiew, Y.M., 2012. Three-dimensional scour at submarine pipelines. J. Hydraul. Eng., 138, 788–795. https://doi.org/10.1061/(ASCE)HY.1943-7900.0000583

Yang, J., Zhang, J., Zhang, Q., Teng, X., Chen, W., Li, X., 2019. Experimental research on the maximum backwater height in front of a permeable spur dike in the bend of a spillway chute. Water. Supp., 19, 1841–1850. https://doi.org/10.2166/ws.2019.061

Zhang, P., Yang, S., Hu, J., Li, W., Fu, X., Li, D., 2020. A new method for extracting spanwise vortex from 2D particle image velocimetry data in open-channel flow. J. Hydrol. Hydromech., 68, 242–248. https://doi.org/10.2478/johh-2020-0020

Received 14 May 2020
Accepted 11 November 2020